THE ASTROPHYSICAL JOURNAL, 418:730–742, 1993 December 1

A COMPLETE CO SURVEY OF M31. I. DISTRIBUTION AND KINEMATICS

T. M. DAME,[1] E. KOPER,[2] F. P. ISRAEL,[2] AND P. THADDEUS[1]
Received 1992 December 23; accepted 1993 June 10

ABSTRACT

The 1.2 m millimeter-wave telescope at the Center for Astrophysics has been used to carry out the first complete CO survey of M31. At 115 GHz, the frequency of the $J = 1 \rightarrow 0$ transition observed, the telescope has a beamwidth of 8.7, corresponding to 1.7 kpc at the distance of M31. A total of 8 hr per day during two 6 month observing periods were devoted to the survey, which covers a $153' \times 45'$ area of the disk with half-beamwidth (4.5) spacing. An average integration time of 100 minutes per point yielded an rms noise of 18 mK in each 1.3 km s^{-1} wide channel of our spectrometer. The entire galaxy has been observed out to a radius of at least 15 kpc—well beyond the optical disk and H I ring.

Like other Population I in M31, the bulk of the CO emission in M31 is confined to a broad ring with a radius of ~ 10 kpc. Secondary enhancements in CO near $R = 4.5$ kpc and 14 kpc, similar to that in other Population I and probably the result of spiral arms, were also detected. The fraction of gas in molecular form drops sharply beyond 10 kpc, but is constant or rising within. Near the tangent of Arp's inner spiral arm N3 at $R = 4.5$ kpc, the H_2/H I surface density ratio is roughly 3 times the mean in the 10 kpc ring.

If the Galactic value for the ratio of H_2 mass to CO intensity is adopted, the molecular mass surface density at the peak of the 10 kpc ring is $\sim 1.3\ M_\odot\ pc^{-2}$, about the same as that in the Milky Way at the same radius, but only one-fifth that at the peak of the Milky Way's molecular ring at 4.5 kpc. Even at the brightest CO positions, the fraction of gas in molecular form appears no larger than one-third. The total H_2 mass of M31 is found to be $2.7 \times 10^8\ M_\odot$, more than a factor of 10 less than that of H I, and about one-fourth the molecular mass of the Milky Way computed in the same way.

Subject headings: galaxies: ISM — galaxies: individual (M31) — galaxies: structure — ISM: molecules

1. INTRODUCTION

As the nearest spiral galaxy to our own, the Andromeda galaxy, M31, has been the most intensely observed of all external galaxies. Its proximity allows studies of its stars, dark clouds, H II regions, and other constituents with resolution achievable in no other spiral except M33. Its high inclination to the line of sight (77°) poses a difficulty in the determination of the distribution of objects in the disk, but it greatly facilitates studies of the disk kinematics.

Although a number of complete 21 cm surveys of atomic hydrogen in M31 have been carried out over the past 30 yr (e.g., Roberts 1966; Emerson 1974; Unwin 1980; Brinks & Shane 1984; Braun 1991), no comparable CO studies of molecular gas have been undertaken. The pioneering study of Combes et al. (1977) showed that CO along the major axis of M31 was confined to the Population I ring about 10 kpc from the galactic center. Strip maps along the minor axis by Stark (1979) and Sandqvist, Elfhag, & Lindblad (1989) confirmed this result and showed that, unlike the center of our Galaxy, the center of M31 contained no significant CO emission. The two largest regions of M31 mapped previously in CO were a $18' \times 15'$ field near the southwest tangent of the Population I ring (Stark, Linke, & Frerking 1981) and a $20' \times 4'$ field in an eastern spiral arm (Ryden & Stark 1986), both studies at an angular resolution of 1.7. Most subsequent CO observations of M31 have been at yet higher angular resolution within one or the other of these two regions, with the purpose of studying the relation of molecular clouds to spiral arms or the properties of individual clouds (see Hodge 1992 for a review).

M31 is difficult to survey in CO in any rotational transition because of its large angular size, roughly 3° by 1°, and the faintness of its CO emission, which in the $J = 1 \rightarrow 0$ line on the scale of 1 kpc is nearly an order of magnitude fainter than that in our own Galaxy. Almost all existing millimeter-wave telescopes have too small a beam, are too insensitive at the CO lines, or are shared by too many observers to fully survey M31 in a reasonable amount of time.

The 1.2 m millimeter-wave telescope at the Center for Astrophysics (CfA) is equipped with one of the most sensitive existing receivers at 115 GHz, the frequency of the CO $J = 1 \rightarrow 0$ line used for most molecular surveys, and this telescope is especially well adapted to large-scale studies requiring months or years of observation. With an 8.7 beam, the CfA telescope has mainly been dedicated to surveys within our own Galaxy, but it has long been apparent that a complete study of CO in M31 with this instrument would be worthwhile, and quite possible with a very sensitive cryogenic receiver. The wealth of useful information on the distribution of gas in M31 that can be obtained at our angular resolution is demonstrated by the 21 cm survey of M31 done with the 100 m Effelsberg telescope (Cram, Roberts, & Whitehurst 1980; hereafter CRW), an instrument with almost exactly the same beam size at 21 cm as that of our telescope at 115 GHz.

Two observing seasons on the CfA telescope, each from autumn to spring, were required to obtain the fully sampled CO survey of M31 presented here. Ours is the first to completely sample the Population I disk of M31, and it provides a linear resolution (1.7 kpc) which is within a factor of a few of that achievable in CO with most filled-aperture telescopes in

[1] Harvard-Smithsonian Center for Astrophysics, 60 Garden Street, Cambridge, MA 02138.
[2] Leiden Observatory, P.O. Box 9513, 2300 RA Leiden, The Netherlands.

other nearby spirals; at M51 even with the IRAM 30 m telescope the linear resolution is ~ 0.6 kpc at the $J = 1 \rightarrow 0$ line, and 0.3 kpc at $2 \rightarrow 1$. Our purpose here is to amplify and extend the brief reports of our survey published recently by Dame et al. (1991) and Koper et al. (1991), presenting maps which summarize the spatial distribution and kinematics of molecular gas in the galaxy, and comparing CO, H I, and other Population I. Further analysis of the survey, including a detailed comparison of the interstellar medium in M31 and the Milky Way using the *IRAS* survey and a discussion of the conversion of CO intensity to H_2 mass in M31 will be presented in Koper et al. (1993; hereafter Paper II).

In the next section we describe the CfA telescope, with emphasis on those components of the instrument, especially its light, rapidly position-switched antenna, computer system, and SIS receiver, which made the survey possible. In § 3 we discuss the observations in detail. In many respects the survey was the most challenging yet undertaken with the 1.2 m telescope, requiring the implementation of new observing techniques and unprecedented care in data acquisition to reduce baseline irregularities. In § 4 we summarize the survey in various ways, including a velocity-integrated spatial map, major axis profile, and position-velocity contours, and compare these to similar displays of the CRW 21 cm survey. We also derive and compare the distributions with galactocentric radius R of H_2 and H I, and their distributions with galactocentric angle around the main gas ring in M31 at $R \approx 10$ kpc.

2. INSTRUMENTATION AND CALIBRATION

The antenna of the 1.2 m telescope, a Cassegrain with a parabolic primary with an rms surface accuracy of 40 μm, and 17.8 cm hyperbolic secondary, is a fast diffraction-limited system with an effective f/D of 3.79. In 1988, a transmitter in the intermediate field at a distance of 1400 m ($2.5D^2/\lambda$) was used to measure the telescope's beam pattern in azimuth and elevation to a radius of 70′, beyond the fourth sidelobes at a power level of -40 dB relative to the main beam. The measured beamwidth at 115 GHz of 8.′7 and beam efficiency of 0.82 were in good agreement with the predictions of scalar diffraction theory. Direct-drive torque motors can position switch the lightweight aluminum antenna over an angle of several degrees to an accuracy of better than 1′ in a time of about 1 s.

The present survey would not have been feasible without the very sensitive SIS heterodyne receiver which was installed on the telescope in 1983. The mixer (an inductively shunted Nb/PbInAu junction; Pan et al. 1989) and the first stage of amplification (a low-noise Weinreb 30 dB high electron mobility transistor [HEMT] amplifier) are maintained at 4 K in a liquid helium dewar. The mixer can be tuned with two backshorts to reject the image sideband to better than 20 dB. Typical single sideband receiver noise temperatures were in the range 60–70 K during the entire present survey. Total system temperatures referred to above the atmosphere ranged from ~ 800 K at the lowest elevations observed ($\sim 30°$) to ~ 400 K at the highest ($\sim 75°$); acceptable weather variations imposed an rms scatter on these values of ~ 25 K. At high elevations, the atmosphere, the far sidelobes, and the receiver made roughly equal contributions to the total system temperature, so a much better receiver would not be of much benefit in Cambridge.

The spectrometer used for our survey, a 256-channel filter bank adapted from an NRAO design (Mauzy 1974), has proved extremely reliable and stable over a decade of use. At 115 GHz, its 0.50 MHz filters provided a velocity resolution of 1.3 km s^{-1}—far better than required for the broad lines observed—and total velocity coverage of 332 km s^{-1}—adequate to cover the full range of 21 cm velocities observed by CRW at any one position while leaving one-quarter to one-half the channels beyond the rotation curve of M31 as spectral baseline. At the sensitivity of the M31 survey, variations in the power-law characteristics of the filters in the spectrometer, particularly systematic variations between groups of 16 filters on a single board, can be a significant source of spurious baseline structure unless residual (ON-OFF) switched power is kept very low. To first order, the amplitude of this effect scales with residual power (Digel 1991), and becomes comparable to the survey rms for residual powers greater than 1 K. To eliminate this effect as a significant source of baseline distortion, residual powers were kept below 0.1 K by the techniques described in § 3.

The first major upgrade of the computer control system of the CfA telescope since its construction in 1974 occurred in the summer of 1990, with the M31 survey half completed. A Data General NOVA computer with 64 kb of random access memory (RAM) and a 5 Mb disk was replaced with a Macintosh IIfx with 5 Mb of RAM and 140 Mb of disk storage. All of the control and data reduction software, originally written in ASSEMBLY language and a customized language similar to FORTH, were simplified and rewritten in C language. The Macintosh communicates with the telescope hardware through a National Instruments 32-bit parallel interface board, and with a Digital Equipment VAXstation II through a serial line. The VAX receives completed spectra from the Macintosh for further processing and can relay messages to observers via electronic mail when problems occur during automated observing. Data can be exported in its original format, along with the new software which can be run on any Macintosh computer, or in FITS format via the VAX. Among the software improvements relevant to the M31 survey were a complete implementation of the (X, Y) offset coordinate mode, allowing mapping and other automated observing procedures, automatic setting of center velocity and baseline windows from CRW data on-line, and more frequent adjustments of the elevation of the OFF position to obtain required low residual switched power (see § 3).

Spectral line intensities were calibrated against a room-temperature blackbody, a standard Eccosorb chopper wheel rotating just in front of the feed horn (Davis & Vanden Bout 1973). Measurements of sky brightness as a function of elevation, obtained at least every 6 hr, were fitted to the two-layer atmospheric model of Kutner (1978) to determine the temperature and opacity of atmospheric water vapor. The ability of the SIS receiver to tune out the image sideband eliminated a serious source of uncertainty in calibrating the CO $J = 1 \rightarrow 0$ line: the significant difference in sky brightness between the image and signal frequencies caused by the pressure-broadened atmospheric O_2 line at 118 GHz. The oxygen opacity at the zenith was assumed constant at 0.378; water opacities ranged from a minimum of 0.05 on the coldest, driest days, to 0.25, the opacity at which observations were abandoned.

All line intensities given here and in Paper II are in units of radiation temperature $T_R = T_A^*/\eta$, where T_A^* is antenna temperature corrected for atmospheric absorption, ohmic losses, and rearward spillover and η is the main beam efficiency given above. Note that intensities reported in Koper et al. (1991) are in units of T_A^*, and thus are lower by a factor of 0.82.

At an angular resolution of 8.'7, there is no strong CO source either in M31 or in the Milky Way near the -300 km s^{-1} systemic velocity of M31. The best that could be found for a check of the intensity calibration and pointing was Galactic source NGC 7538 at $v = -55$ km s^{-1}, 24° away at $l = 111.°5$, $b = 0.°75$. Since the CO frequency of NGC 7538 is 100 MHz or more from that of the gas in M31, it was necessary to retune the SIS receiver, remeasure its receiver temperature, and recalibrate the atmospheric model between observations of the test source and M31. This procedure was performed twice daily, once at the start of observations, and again 6 hr later, following a 2 hr period during which M31 was too close to the zenith to be tracked by the altitude-azimuth mount. The mean velocity-integrated CO temperature of NGC 7538 (in the range -90 to -30 km s^{-1}) was 121 K km s^{-1}, with a day-to-day variation of less than 3% rms.

3. OBSERVATIONS

Even when observed on an angular scale of $\sim 1'$, CO lines in M31 are weak (<0.1 K) and broad ($\Delta v \sim 50$ km s^{-1}: e.g., Ryden & Stark 1986; Blitz 1985). With a small dish, beam dilution tends to weaken the velocity-integrated line intensity, and velocity gradients across the beam widen the lines and further reduce the peak line intensity. Because, as discussed below, we observed a given position in M31 for no longer than ~ 20 minutes on any given day, the survey was conducted "blind" in the sense that lines could not be discerned in individual spectra. It was therefore necessary to take great care to ensure that the telescope was operating properly. Even when many spectra were summed, extremely flat baselines, free of systematic errors, were required to detect the very broad lines observed at our angular resolution.

November to April is generally the best observing period in Cambridge, and the present survey was done during those months in 1989–1990 and 1990–1991. M31 was observed daily, weather permitting, for 8 of the 10 hr when it was above an elevation of 35°. Observations could be made on roughly half the days during each period. Clear skies were generally required when the outside temperature was above freezing; below freezing some diffuse cirrus clouds were tolerable.

To randomize possible systematic errors, observations of a given point in M31 were divided among 5 separate days normally separated by weeks or months. Each observation was to an rms noise of 40 mK per channel and typically required 20 minutes of integration. Averaging the five observations yielded an overall noise level of 18 mK. On a given day, observations were confined to one or two groups of points which were close in radial velocity (± 25 km s^{-1}), to maintain optimum receiver tuning, but well distributed spatially, to randomize slight calibration differences from day to day.

The 21 cm survey of CRW was extremely useful in guiding the observations, since on the scale of our beam CO and H I are fairly well correlated in M31. We observed a total of 365 positions lying on exactly the same half-beamwidth (4.'5) rectangular grid as that of CRW, centered at $\alpha = 0^h40^m$, $\delta = 41°$ (1950), with X increasing toward the northeast along the major axis of M31, at position angle 38°, and Y increasing along the minor axis toward the southeast.[3] Our observations cover just over 2 deg^2, and include all of the area within 16 kpc of the center of M31, and 70% of the area between 16 and 21 kpc from the center. At each position, the spectrometer was centered on the emission-weighted mean H I velocity from CRW, and only those channels at velocities where T_A(H I) < 1 K (i.e., less than 10% of typical peak H I intensities) were used in removing linear baselines from the spectra.

Cautioned by the fact that the first reported detection of CO in M31 was entirely spurious (Solomon & de Zafra 1975; their claimed line toward the galactic center turned out to be baseline ripple with a velocity-integrated intensity ~ 100 times that of subsequent upper limits set at that position, as shown by Rickard et al. 1977 among others), we took several unusual steps to ensure flat spectral baselines. Azimuth switching to a point just outside the H I disk of CRW ($|X| > 130'$ or $|Y| > 45'$) was used to remove most of the instrumental baseline distortion. We further adopted a full switching period of 20 s, shorter than the 30 s period usually employed, to reduce short-term sky and gain variations. Since M31 lies more than 20° from the Galactic plane, foreground Galactic emission is not expected near -300 km s^{-1}, and there is no evidence for high-velocity CO in M31 which could be confused with Milky Way CO near 0 km s^{-1}. Velocities over the main gas ring of M31 range from -550 km s^{-1} at the southwest limb to -50 km s^{-1} at the northeast limb (see Fig. 1 of Koper et al. 1991).

The reference (OFF) position, typically displaced from the source (ON) position by 1°–2° in azimuth, was also displaced by a few arcminutes in elevation to cancel small shifts in total power with azimuth. Since the OFF is always observed 10 s after the ON, the $\sim 2'$ change in elevation of M31 during that time will introduce a systematic difference in total power between the ON and OFF of ~ 0.1 K. To cancel this difference, the OFF was displaced 2.'1 below the ON while M31 was rising, and the same distance above while setting.[4] Although this resulted in residual powers which were very small, clouds and instrumental fluctuations introduced an rms scatter in the residual powers of ~ 0.2 K. A comparable scatter resulted even if the ON and OFF were held at the same fixed position on the sky.

To cancel these random variations in total power, the elevation of the OFF relative to the ON was periodically adjusted during an observation. The adjustments were made 8 times per scan during the first observing season and more frequently (every ON-OFF cycle) during the second season. At the time of an adjustment, the calibrated atmospheric model of Kutner (1978) was used to calculate the elevation offset necessary to cancel the current residual power by the end of the scan. Offsets were kept below 10′ to avoid accidentally switching too close to the disk of M31, but generally offsets of only 2′–3′ were sufficient to balance total powers at the ON and OFF to better than 1 part in 10^4. The average residual power for all scans in the survey is 0.02 K, with a scan-to-scan variation of 0.05 K rms. A small fraction of scans ($\sim 5\%$) with residual powers greater than 0.1 K were repeated; these were generally from days when clouds produced larger and more rapid total power variations than normal.

It does not appear that residual baseline curvature or ripple contributes significant systematic errors to the survey, even to velocity-integrated maps which are the most sensitive to wide spurious spectral features. The observed rms noise calculated over all baseline channels is consistent with that expected from purely statistical instrumental noise. Figure 1 demonstrates

[3] The λ, β coordinate system of CRW is defined such that $\lambda = X$ and $\beta = -Y$. Our coordinate system is negligibly different from that defined by Baade & Arp (1964).

[4] The value 2.'1 assumes a constant rise/set rate of 0.'18 s^{-1} and an average observing efficiency of 88%.

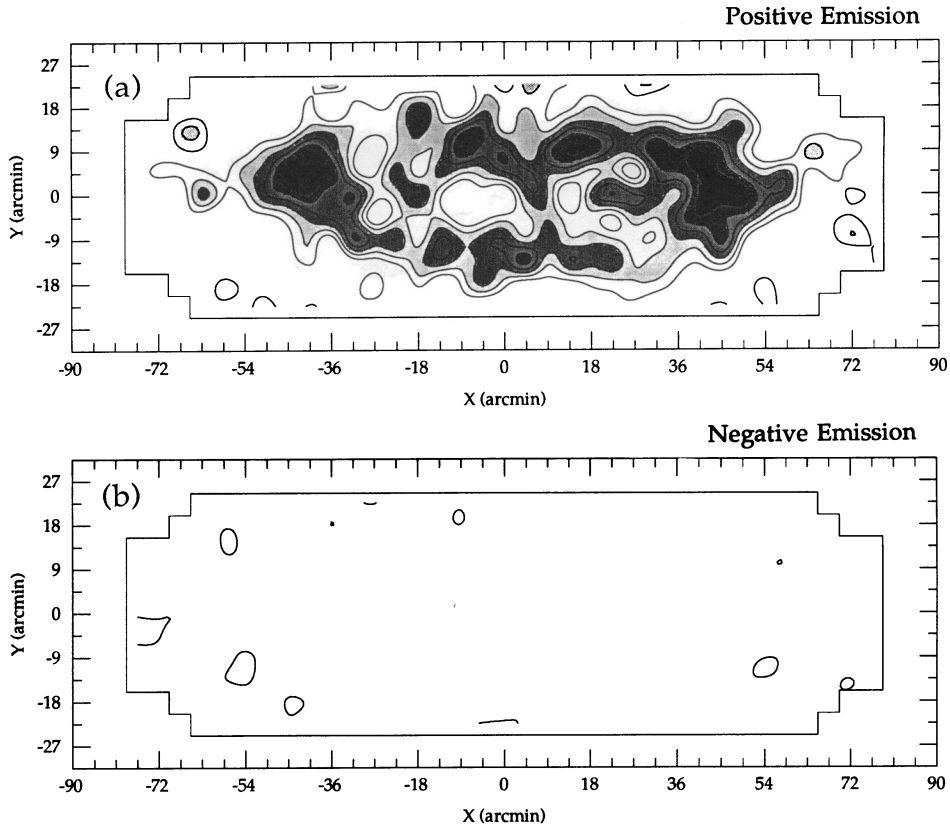

FIG. 1.—Velocity-integrated CO emission, W_{CO}, in M31. (*a*) Positive emission, with the contour interval and lowest contour at 0.19 K km s^{-1}, about the 1 σ noise level. (*b*) Negative emission similarly contoured, a demonstration that little of the structure in (*a*) is the result of noise.

clearly that the positive emission contoured in (*a*) lies well above the noise, since little negative emission is seen in (*b*). Further, the noise around the edges of the map, where there is little or no emission, is close to that expected. This point is demonstrated quantitatively in Figure 2, which compares the distribution of W_{CO} values around the edges of the map with that expected. A χ^2 test indicates that the two distributions are indistinguishable at the 98% confidence level.

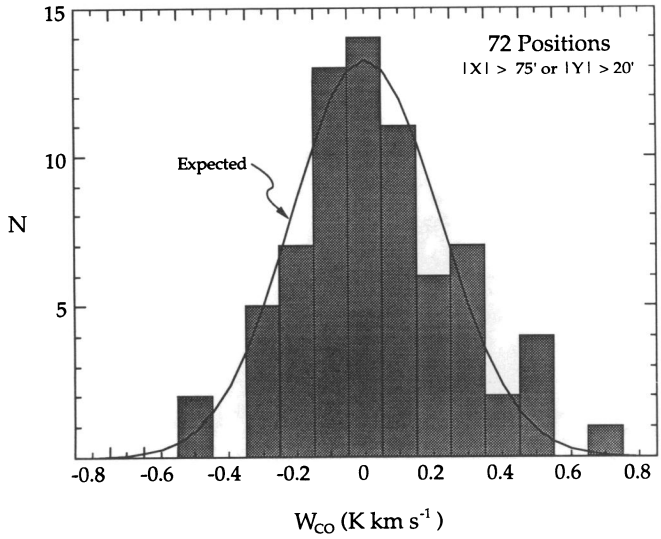

FIG. 2.—Histogram of W_{CO} in regions thought to be free of CO: the 72 positions surveyed at $|X| > 75'$ or $|Y| > 20'$. The smooth curve shows the distribution expected from purely statistical instrumental noise.

4. DISCUSSION

4.1. W_{CO} Map

In the Milky Way, the velocity-integrated CO intensity, W_{CO}, is the most useful and widely used tracer of total molecular mass, i.e., the molecular hydrogen column density $N(H_2)$. Independent estimates of H_2 mass based on (i) the virial theorem (Solomon et al. 1987), (ii) extinction in the visual and near-IR (Dickman 1978; Dame 1993), and (iii) high-energy gamma rays (Strong et al. 1988) demonstrate that W_{CO} is a particularly good tracer of H_2 on the scale of giant molecular clouds (GMCs) or larger, and all three estimates yield a mass calibration $X \equiv N(H_2)/W_{CO}$ of about 2×10^{20} cm^{-2} K^{-1} km^{-1} s. Because the beam of the 1.2 m telescope subtends such a large area at the distance of M31, it is likely that as here, W_{CO} is a good tracer of H_2 mass in M31, but there is no assurance that X is the same as here. For the sake of comparison with most Galactic and extragalactic work to date, we will adopt the Galactic value of X derived by Strong et al. (1988) from an intercomparison of CO, H I, and gamma-ray surveys[5] and defer discussion of the best value to adopt for X in M31 to Paper II.

The most important result of the present survey, the distribution of W_{CO} across M31, is shown in Figure 3*b* along with similar maps of other Population I. The noise in the W_{CO} map has been somewhat reduced by degrading the angular resolution slightly (to 10′) by convolution with a Gaussian smoothing function with a width approximately equal to that

[5] Scaled down by 22% to 1.9×10^{20} cm^{-2} K^{-1} km^{-1} s to account for a calibration difference between the T_R scale used here and that used by Strong et al. (see Bronfman et al. 1988 for details).

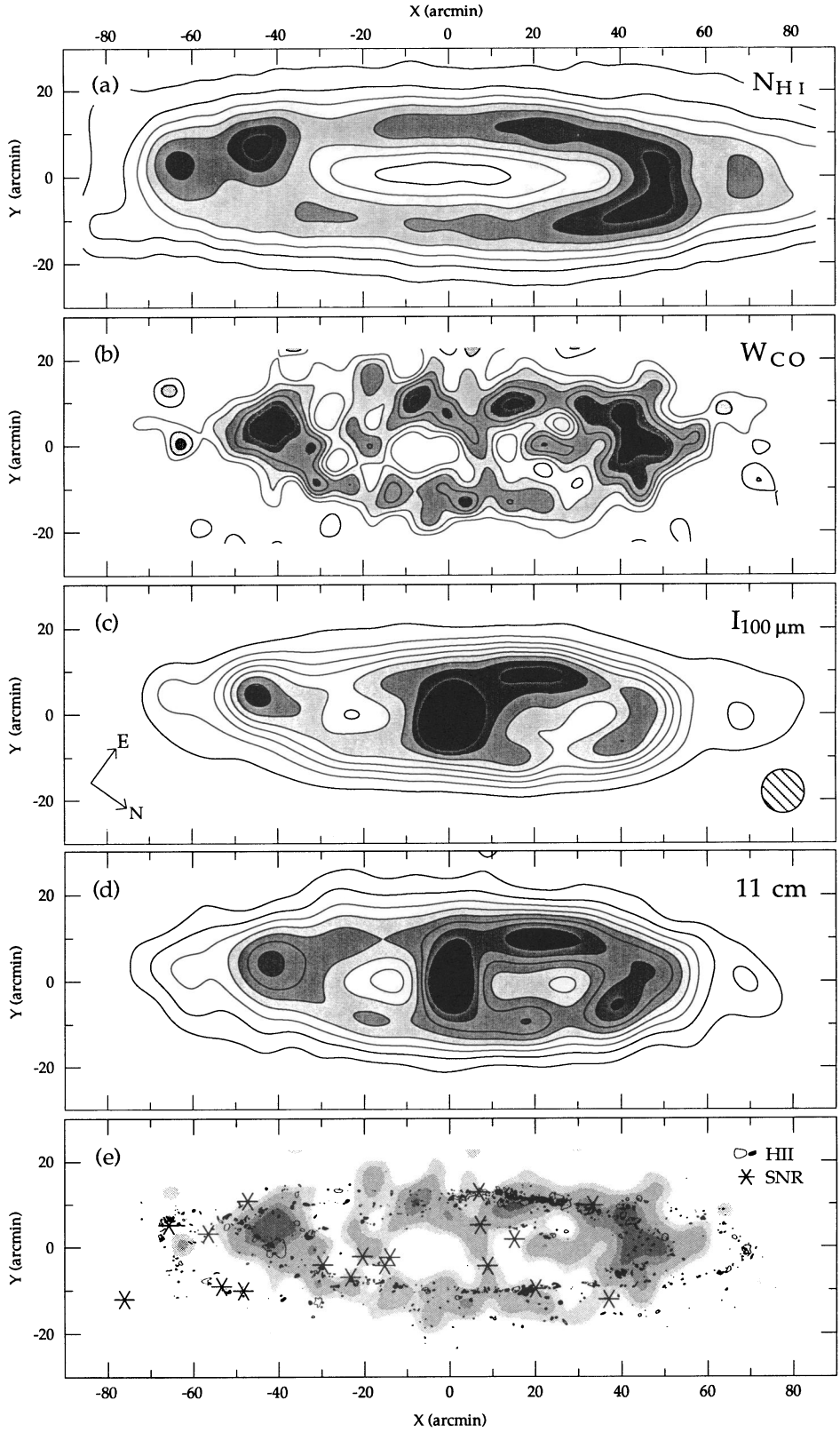

FIG. 3.—Spatial maps of Population I in M31. X and Y are rectangular offsets from $\alpha = 0^h40^m$, $\delta = 41°$ along and perpendicular to the major axis, at position angle 38°. Maps *a–d* are spatially smoothed to an angular resolution of 10′, the cross hatched disk in Fig. 3*c*. (*a*) H I column density derived from the 21 cm survey of Cram, Roberts, & Whitehurst (1980) with foreground emission from the Milky Way removed; the contour interval is 3.4×10^{20} cm^{-2}. (*b*) Velocity-integrated CO intensity, from Fig. 1*a*. (*c*) *IRAS* 100 μm emission; the contour interval is 1.8 MJy sr^{-1}. (*d*) Continuum map at 2695 MHz from the survey of Beck & Gräve (1982); the contour interval is 6.5 mK. Strong point sources with flux density greater than 11 mJy have been removed. (*e*) The positions of optical H II regions and supernova remnants overlaid on the W_{CO} map, shaded as in (*b*). The H II regions are from Fig. 2 of Pellet et al. (1978), the brighter ones in black; the SNR are from the catalog of D'Odorico et al. (1980).

of the half-beamwidth sampling interval. Each of the other Population I maps shown in Figure 3 has been smoothed to the same resolution. The only significant differences between Figure 3*b* and the W_{CO} map presented by Koper et al. (1991) occur at the adjacent positions $(X, Y) = (22.5, 0)$ and $(27, 0)$. Two distinct H I lines of comparable strength at each of these locations (see Fig. 7 below) resulted in inappropriate choices for CO baseline windows at these positions in the Koper et al. map. All other baseline windows were rechecked to ensure that similarly poor baseline fits did not occur elsewhere in the survey.

Figure 3*a* is the atomic hydrogen column density derived from the survey of CRW on the assumption that the 21 cm line is everywhere optically thin. The H I data of CRW used throughout this paper has been corrected for Galactic foreground emission, which is significant at $X \geq 13'.5$. Since the foreground emission appears to vary smoothly with Y (see, e.g., Fig. 3 of CRW), it was removed at each X by fitting a straight line to the emission at large $|Y|$. CRW used a similar technique in producing their velocity-integrated map (cf. their Fig. 6*g*), which agrees extremely well with Figure 3*a*.

Figure 3*c* is the 100 μm map derived from *IRAS* "additional observations" taken on a regular grid toward M31; the original map had a resolution of $6'.9 \times 4'.3$, with the long axis of the beam roughly aligned with the major axis of the galaxy (Walterbos & Schwering 1987). Figure 3*d* is the 11 cm continuum map; strong point sources were removed, since $\sim 90\%$ of them are expected to be from background objects unrelated to M31 (Berkhuijsen 1977). The W_{CO} shading is repeated without the contours in Figure 3*e*, with the positions of optical H II regions and supernova remnants overlaid.

In CO as in other Population I, the largest scale structure evident in M31 is a fairly well-defined ring with a radius of ~ 10 kpc. A similar distribution of molecular clouds and other Population I is observed in our Galaxy, and indicates that in M31, as here, molecular clouds as traced by CO are the probable precursors to the star formation manifested in various ways in Figures 3*c*–*e*: young massive stars born in molecular clouds produce the H II regions (Fig. 3*e*), the 100 μm emission (Fig. 3*c*) through dust heating, and the thermal component of the 11 cm continuum (Fig. 3*d*). The nonthermal continuum, which Berkhuijsen & Wielebinski (1974) estimate accounts for approximately half the total at 11 cm, also derives at least in part from molecular clouds, since Type II supernovae descended from massive stars generate the cosmic-ray electrons responsible for the nonthermal synchrotron radiation. In M31, as in the Milky Way, the molecular ring is resolved at higher resolution than ours into spiral arms (e.g., Braun 1991), and is therefore not at all axisymmetric on the scale of ~ 1 kpc and smaller.

A number of differences between the maps in Figure 3 are worth noting. Even at our limited resolution, it is evident that in CO M31 is about the same size as in other Population I tracers, except H I, in which it is significantly larger. The strong H I peaks along the major axis at $X = -63'$ and $X = 70'$ correspond to the tangent regions of the optical spiral arms S5 and N5, respectively (Arp 1964). Surprisingly, these outer arms have a relatively high density of optical H II regions, even though they are weak in CO, far-infrared, and radio continuum. The reason for this is unclear; it may be because optical H II regions are easier to detect beyond the crowded and dusty Population I ring.

The strong far-infrared and radio continuum emission at the center of M31 is somewhat surprising, given the absence there of appreciable gas and star formation. Although neither emission is entirely understood, both probably derive from the high density of old stars in the center: the far-infrared from dust heated by late-type giants (Habing et al. 1984) and the radio continuum from Type I supernovae (Walterbos 1986; Hjellming & Smarr 1982). The lack of a clearly defined 10 kpc ring in the distribution of optical supernova remnants (Fig. 3*e*) is also somewhat surprising, but may simply be the result of the higher obscuration in the ring.

4.2. *Azimuthal Distribution*

Since much of the CO, H I, and 100 μm emission in M31 lies in a fairly narrow ring, a useful quantitative intercomparison can be obtained by plotting the mean ring intensity in each tracer as a function of galactocentric azimuth φ. The curves in Figure 4 represent mean face-on intensity in 10° slices of galactocentric azimuth bounded by galactic radii 6 and 14 kpc (30′ to 70′ along the major axis). With the data transformed in this way, the pronounced limb brightening seen in the W_{CO} map along the major axis is removed.

Except in the region from $\varphi = 300°$ to 320° to be discussed below, CO, H I, and I_{100} around the Population I ring correlate fairly well. However, the amplitude of the variations in CO is much larger than that of H I: the brightest and weakest sections of the ring differ in CO intensity by a factor of ~ 6, but

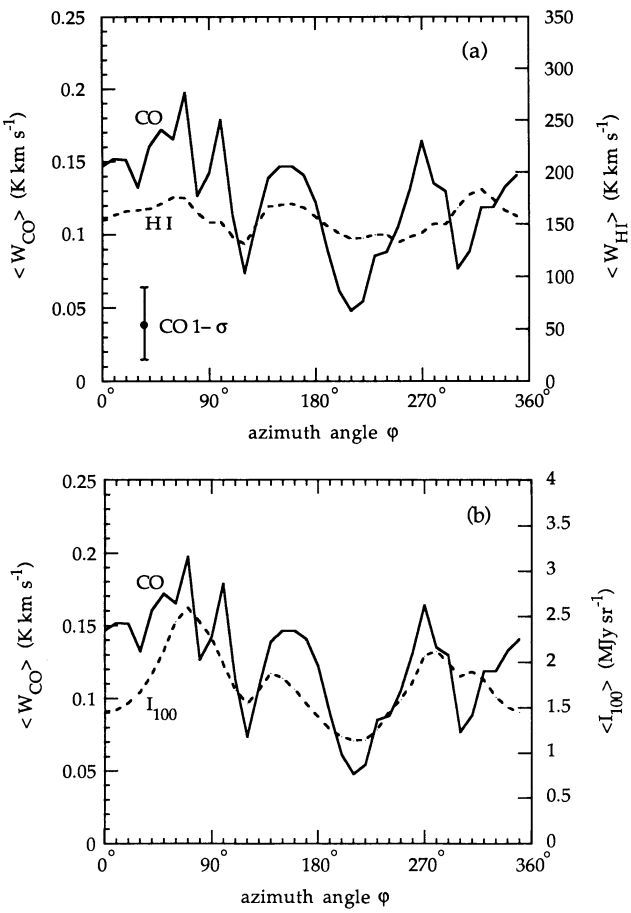

FIG. 4.—Mean face-on CO intensity in 10° slices of galactocentric azimuth φ bounded by galactic radii 6 and 14 kpc (30′ to 70′ along the major axis). CO is compared to the corresponding H I and 100 μm intensities in (*a*) and (*b*), respectively.

only by ~30% in H I. It is evident from the size of the CO error bar that this difference is not attributable entirely to noise in the CO data. Interpretation of this variation around the ring is complicated by the finite thickness of the disk—probably larger for H I than for CO—which folds in a significant amount of gas outside the nominal 6–14 kpc radius (Boulanger, Stark, & Combes 1981). Still, given the high contrast of CO as a spiral arm tracer in external spirals (see Casoli 1991 for a review) and the Milky Way (Dame et al. 1986; Grabelsky et al. 1988), it is possible that the larger variations for CO reflect a higher arm-interarm contrast of molecular gas in M31 relative to that of the atomic gas. As will be shown in Paper II, I_{100} correlates fairly well with total gas density in M31, so it is not surprising that its variation in intensity around the ring lies between that of CO and H I.

It is worth noting in Figure 4 that the Population I ring at the northeast tangent at $\varphi = 0°$ ($X = 45'$, $Y = 0'$) is not particularly bright in CO, and actually appears as a shallow minimum in H I and I_{100}. The southwest tangent is expected at $\varphi = 180°$, but the spatial map (Fig. 3*b*) suggests that the ring may be warped in this region, since a peak quite similar to that of the northeast tangent appears ~4′ above the major axis at $X = -45'$. This region appears at $\varphi = 150°$ in Figure 4 and is bright in all three tracers.

Two significant gaps and one strong peak in the molecular ring also appear in the other Population I in Figure 4. The gaps occur on either side of the southwest tangent, at $\varphi = 210°$ and 120° (corresponding roughly to [−35′, −7′] and [−27′, +9′] respectively in the spatial maps). The gap at (−27′, +9′) is evident in the spatial distributions of all Population I in M31, even SNRs (Fig. 3*e*). Features worth pointing out in this region are a large-scale irregularity in the magnetic field (Berkhuijsen, Beck & Gräve 1987) and a far-infrared spur extending above this irregularity to $Y > 30'$ (Walterbos & Schwering 1987). The brightest section of the ring in CO and I_{100}, and the second brightest in H I is centered at $\varphi = 70°$ and corresponds to a spiral arm in the eastern quadrant (22.5, 9′) previously mapped by Ryden & Stark (1986). This region is the brightest in the 11 cm spatial map (Fig. 3*d*), brighter even than the limb-brightened tangents, and is the richest in H II regions (Fig. 3*e*).

It is rather surprising that the brightest section of the ring in H I, centered at $\varphi = 315°$, is not prominent in other Population I. The CO has a broad minimum through this region, with a deep though narrow gap at $\varphi = 305°$. In the spatial maps (Fig. 3) all of the tracers except H I show a gap in this section of the ring (near 30′, −10′). This gap is also quite evident in the map of warm dust derived by Walterbos (1986), but much less so in his map of cool dust. It would be worthwhile to compare this region in detail with the eastern arm region discussed above, since both have comparable amounts of H I but differ markedly in CO emission and star formation.

4.3. *Major Axis Profiles*

The major axis profiles in Figure 5 exhibit directly the radial distributions of CO, H I, and far-infrared emission in M31. A determination of the radial distribution of CO from all of the survey data is given in Section 4.6, but that along the major axis alone gives the radial distribution so directly that it is worth discussing first. Major axis profiles are of additional interest because there are several regions of substantial CO emission inside the Population I ring which happen to lie along the major axis.

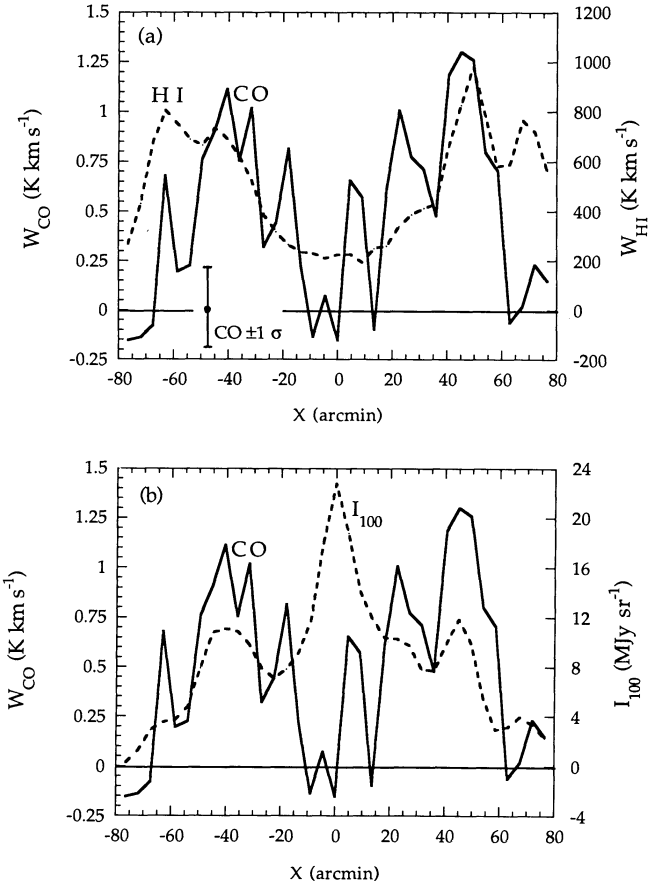

FIG. 5.—Integrated intensity of CO along the major axis, compared with that of H I (*a*) and 100 μm (*b*). For all three tracers, the intensities are those at $Y = 0'$, after smoothing to an angular resolution of 10′ as in Fig. 3.

The CO and H I major axis profiles in Figure 5 differ slightly from those in Figure 3 of Koper et al. (1991) in three ways: (i) most importantly, the Koper et al. profiles assume that the southwest side of the disk is warped, the major axis passing through the strong emission peak at (−45′, 4.5), while the profiles here are strictly at $Y = 0'$; (ii) the revised spectra at (22.5, 0) and (27, 0) discussed in § 4.1 produce a peak which is not in the Koper et al. profiles; and (iii) the Koper et al. profiles are an average over a 9′ strip of Y, while the profiles here display the $Y = 0'$ positions from the W_{CO} map (Fig. 3*b*), which has been smoothed to 10′ resolution.

As Figure 5 shows, CO, H I, and 100 μm emission along the major axis are all fairly symmetrical about the galactic center. The opposite sides of the Population I ring, at ±45′, are nearly equal in intensity in all three. The opposing spiral arms S5 (−63′) and N5 (70′) are also evident in all three tracers, although most pronounced in H I. On the other hand, the main spiral arms inward of the ring, S3 and N3 near ±25′, are not obvious in H I, but peaks possibly related to both these arms exist in CO, and there is one near N3 in I_{100}.

Because of the strong concentration of CO and other Population I in the 10 kpc ring, one might expect the fraction of gas in molecular form to be highest there, but there is some evidence to the contrary. Figure 6, which was derived directly from the curves in Figure 5 using the Milky Way value for the H_2 mass to CO intensity ratio, X, shows the ratio of molecular

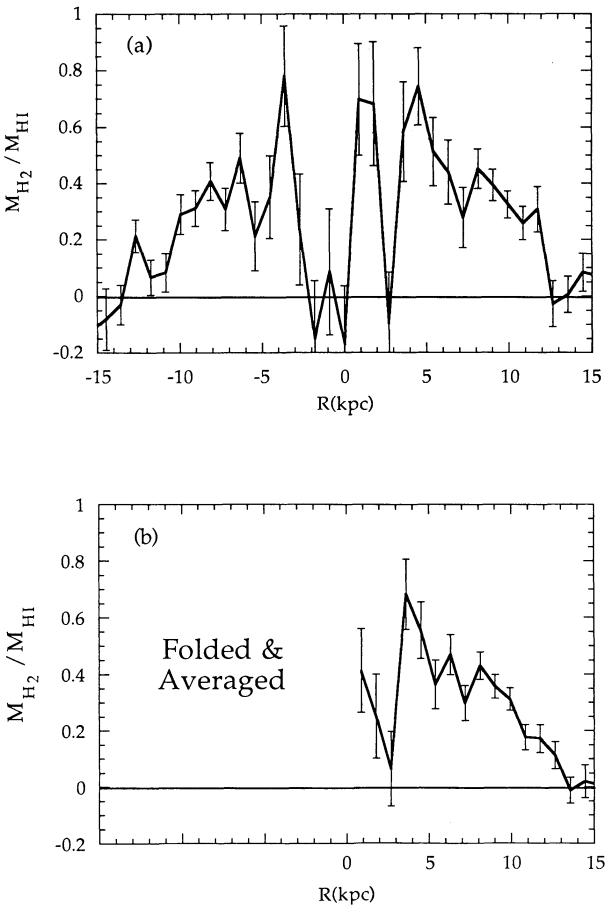

FIG. 6.—The ratio of molecular to atomic mass surface density as a function of position along the major axis, derived directly from the observed CO and H I intensities shown in Fig. 5, assuming the Milky Way value for the $N(H_2)/W_{CO}$ ratio (see text). In (*b*), the profile has been folded about $X = 0'$.

to atomic gas mass as a function of position along the major axis. On both sides of the center there is a relatively smooth increase in the molecular fraction with decreasing radius, from a value consistent with zero at $|R| > 14$ kpc to ~40% near ±4 kpc. A radial decrease in X, as suggested by the results of both Paper II and Allen & Lequeux (1993), would imply an even steeper increase in the molecular fraction with decreasing radius. The Population I ring, so prominent in the CO and H I spatial maps (Fig. 3), is little evident in Figure 6. The increase in the molecular fraction from the outer to the inner edge of the ring is fairly distinct even in the major axis profiles of CO and H I (Fig. 5), where the CO is seen to peak ~5′, or 1 kpc, inward of the H I.

This evidence for an increase in the molecular gas fraction inward of the Population I ring must be considered tentative, since it largely depends on only a few, rather small emission regions (§ 4.4) lying along the major axis. As shown below (§ 4.6), a more sophisticated analysis of the radial distributions of CO and H I based on all our data, not just that along the major axis, does not show as distinct a rise in the molecular fraction with decreasing radius. Still, the existence of even a few positions with a molecular fraction higher than that in the Population I ring is worthy of notice, because each position is an average over such a large area of the galactic disk (~13 kpc^2). It is worth noting in this regard that CO observations of M31 made with the Bell Laboratories 7 m antenna have already confirmed that the tangent of Arp's arm N3 at $R \sim 5$ kpc is brighter in CO than the tangent of the Population I ring at 10 kpc (Bally 1992).

4.4. *Particular Regions*

As in the Milky Way, it is evident from Figure 3 that the molecular ring in M31 is extremely irregular, possessing a great deal of azimuthal structure presumably the result of spiral arms. To partition the CO emission into spiral arms in a credible way requires higher angular resolution than ours, and that will not be attempted in this paper or its sequel, but it is still worthwhile to discuss individually the large regions of enhanced CO emission evident in Figure 3. For the sake of this discussion we will dissect the molecular gas in M31 into the 19 regions shown in Figure 7, *without the implication that any physical interaction or order, gravitational or otherwise, is responsible for this segregation*—these regions are generally far too big to be molecular clouds or even cloud complexes, so it would make no sense to attempt to estimate masses for any of the regions from the virial theorem. Several of the regions, however, may *mainly* consist of segments of particular spiral arms. Composite CO and H I spectra were produced for each of the regions, and some of the more interesting of these are shown in Figure 7. The composite spectra are useful for displaying the signal-to-noise ratio for discrete CO features, the quality of the spectral baselines, and the correspondence of CO and H I emission lines. Data determined from Gaussian fits to the CO composite spectra—peak temperature, velocity, and linewidth—as well as positions and other data for each region are given in Table 1.

The variation in the CO/H I ratio across the disk of M31 is readily apparent from the sample composite spectra in Figure 7, all plotted to the same scale. The regions which lie squarely in the Population I ring, i.e., 2, 8, 13, 16, and 17, are rather similar in CO and H I. In contrast, the H I lines for regions 5 and 14, which lie well within the ring, are weak, yet the mean CO peak temperature of region 14 is the highest of any region in the survey. Region 5 is much weaker in CO, and may consist of two separate velocity components separated by roughly 100 km s^{-1}. These two components are marginally seen with poor signal-to-noise ratio at each of the two observed positions which compose region 5. As the scaled (dotted) version of the H I spectrum shows, both CO lines have H I counterparts, and the H I spectrum shows another intermediate component as well.

4.5. *Velocity Structure*

Since most of the CO emission we detected lies either in the 10 kpc molecular ring, which is only one or two beamwidths wide in our survey, or along the major axis, most of the velocity information contained in the survey can be summarized by three X-v contour maps, one integrated over the southeast ($Y > 0'$) portion of the ring (Fig. 8*a*), one at $Y = 0'$ (Fig. 8*b*), and one over the northwest ($Y < 0'$) portion of the ring (Fig. 8*c*). The H I emission for the same regions are shown by the dotted contours. For better comparison, both the CO and H I contours are linearly spaced, except that an additional, very low-intensity contour is added for the H I to outline the full extent of the atomic gas.

As the numbers in Figure 8 show, nearly all of the discrete emission regions evident in the spatial map (Fig. 7) are also well-defined in velocity, and generally show a good correspon-

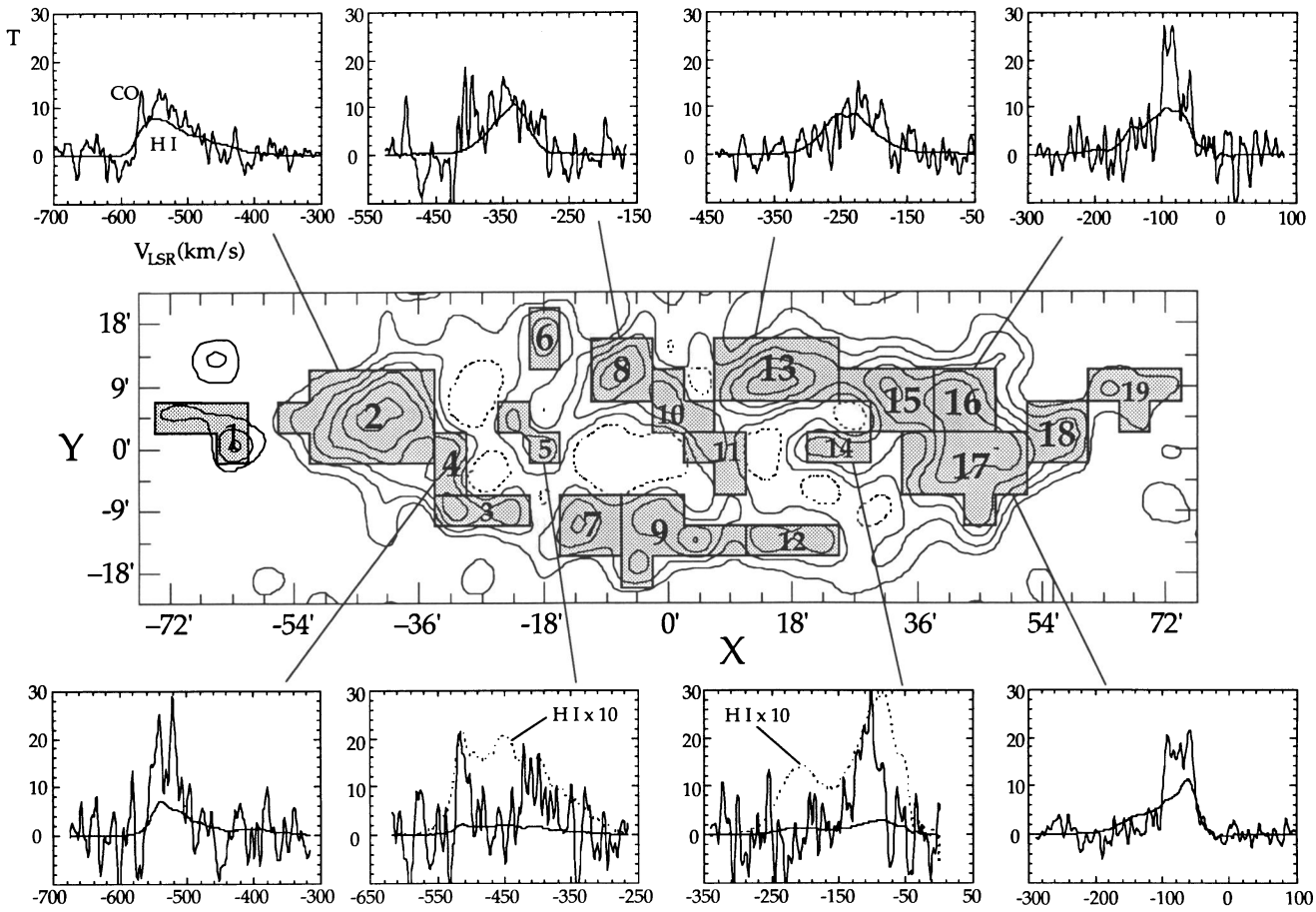

FIG. 7.—Boundaries of the CO emission regions compiled in Table 1, overlaid on the W_{CO} map from Fig. 3*b*. Averaged CO spectra from the present survey (T_R) and 21 spectra from the CRW survey (T_A) are shown for some of the regions. Each spectrum has the same temperature and velocity scale, but the CO temperature is scaled up by a factor of 1000 in each. The dotted curves in the composite profiles of regions 5 and 14 are the 21 cm spectra scaled up by a factor of 10.

TABLE 1

CO EMISSION REGIONS IN M31

Region	*X*	*Y*	*R*	*N*	*T*	*v*	Δv	σ_{H_2}	$\sigma_{H\,I}$	$\sigma_{H_2}/\sigma_{H\,I}$	Comments
1	−63.00	0.00	12.66	4	7.9	−544	49.8	0.31	2.34	0.13	Arp outer arm S5
2	−40.50	4.50	9.08	13	11.8	−533	69.8	0.64	2.60	0.25	SW tangent of population I ring
3	−31.50	−9.00	10.23	3	11.6	−462	60.6	0.68	2.31	0.29	
4	−31.50	0.00	6.33	2	19.9	−529	45.4	0.66	1.93	0.34	Inner edge of SW tangent
5	−18.00	0.00	3.62	2	12.0	−406	49.6	0.67	1.03	0.65	Possibly tangent of Arp arm S3
					20.3	−512	16.2	...	...		Second velocity component of region 5
6	−18.00	18.00	16.48	2	9.5	−373	95.6	0.58	1.69	0.35	Weak feature at suspiciously large *Y*
7	−13.50	−9.00	8.49	4	6.4	−366	101.1	0.51	2.10	0.24	
8	−9.00	9.00	8.24	4	11.8	−350	86.0	0.69	2.37	0.29	
9	4.50	−13.50	12.10	7	7.7	−322	83.9	0.53	2.10	0.25	Along NW minor axis
10	0.00	9.00	8.04	3	12.6	−312	71.7	0.64	1.45	0.44	Along SE minor axis
11	4.50	0.00	0.90	3	8.3	−248	67.9	0.46	0.79	0.58	Weak "bridge" near minor axis
12	13.50	−13.50	12.36	3	12.0	−252	51.0	0.60	2.42	0.25	
13	13.50	9.00	8.49	8	10.3	−220	71.0	0.56	2.66	0.21	Spiral arm mapped by Stark et al. (1981)
14	22.50	0.00	4.52	2	24.1	−106	37.4	0.66	1.13	0.58	Near tangent of Arp arm N3
15	31.50	9.00	10.23	5	12.4	−119	61.3	0.68	2.59	0.26	Extension of eastern arm
16	40.50	9.00	11.44	4	22.3	−86	40.7	0.78	2.85	0.27	Highest H_2 mass surface density
17	45.00	0.00	9.05	9	19.7	−74	47.2	0.71	2.63	0.27	NE tangent of population I ring
18	54.00	0.00	10.85	4	11.5	−52	43.5	0.48	2.27	0.21	Outer edge of NE tangent
19	63.00	9.00	15.00	4	6.9	−48	38.5	0.25	1.48	0.17	Arp outer arm N5

NOTE.—*X*, *Y* = rectangular offsets from $\alpha = 0^h40^m$, $\delta = 41°$ (arcmin); *R* = galactic radius of peak position (kpc); *N* = number of observed points in region; *T* = peak temperature from Gaussian fit to composite profile (mK); *v* = mean LSR velocity from Gaussian fit to composite profile (km s^{-1}); Δv = FWHM line width from Gaussian fit to composite profile (km s^{-1}); σ_{H_2} = mean H_2 mass surface density ($M_\odot$ pc^{-2}); $\sigma_{H\,I}$ = mean H I mass surface density ($M_\odot$ pc^{-2}); $\sigma_{H_2}/\sigma_{H\,I}$ = molecular-to-atomic mass surface density ratio.

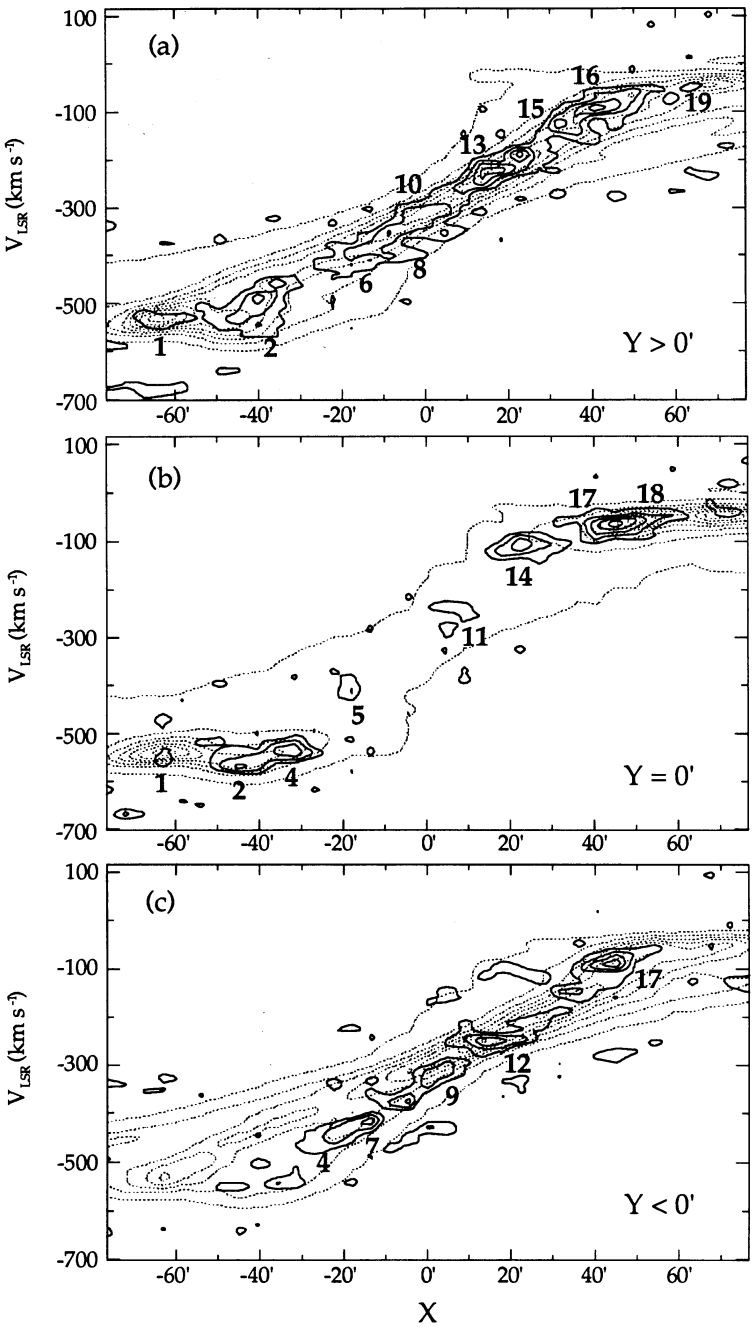

FIG. 8.—Contour maps of CO (*solid*) and 21 cm (*dotted*) intensity as a function of X and LSR velocity: (*a*) integrated from $Y = 2'.25$ to $15'.75$, (*b*) integrated from $Y = -2'.25$ to $2'.25$, and (*c*) integrated from $Y = -15'.75$ to $-2'.25$. The CO contours have been smoothed to a resolution of 10′ by 20 km s^{-1}. In (*a*) and (*c*), the CO contour interval is 0.05 K arcmin and the H I contour interval is 20 K arcmin, with one additional contour at 3 K arcmin. In (*b*), the CO contour interval is 0.03 K arcmin and the H I contour interval is 12 K arcmin, with one additional contour at 1 K arcmin. The numbers refer to the emission regions identified in Fig. 7 and listed in Table 1.

dence with H I. This provides additional evidence that most of the CO features in the W_{CO} map are real, and that contamination by baseline ripple or curvature is small or negligible. Note in particular the weak CO features near $X = \pm 65'$ in Figures 8*a* and 8*b*, which may correspond to the outer spiral arms S5 and N5. Although these CO features are only a few standard deviations above the instrumental noise, their close correspondence with H I is additional evidence for the detection of some molecular gas beyond the Population I ring. Note also how weak these features are relative to region 14 (Fig. 8*b*), even though they lie in regions with much more H I (see § 4.3).

The CO emission is generally less extended in velocity than the H I, with only one velocity component at locations where the H I has two or more. This is possibly entirely the result of the lower dynamic range of the CO data: a more sensitive survey might reveal the other components. At $|X| > 30'$, where the H I lines are broad and complex, the CO line generally lies near the most extreme velocity H I component, i.e., that far-

thest from the systemic velocity of the galaxy and arising from the inner disk. The good correspondence of CO and H I at the extreme velocities is also evident in Figure 1 of Koper et al. (1991), which compares CO and H I composite spectra from the Population I ring. There is little CO emission associated with the other main H I component—that at less extreme velocities which is generally attributed to the warped outer disk of the galaxy (e.g., Henderson 1979).

4.6. *Radial Distribution*

Determining the radial distribution of CO emission in M31 is difficult because of the galaxy's high inclination, only 13° from edge-on. Since the beam of the CfA telescope is 1.7 kpc in diameter at the distance of M31, and its projection onto the disk is 7.6 kpc in the Y direction, a simple binning of emission in radius yields a radial distribution with a resolution much worse than that of the beam along the major axis. The best way to determine the mean molecular distribution is by model fitting.

We have used the Richardson-Lucy (R-L) iterative rectification scheme (Lucy 1974) to determine the radial distribution which best reproduces the observed map. This Bayesian technique differs from the methods of χ^2 minimization and maximum likelihood in that it conserves the constraints on frequency distributions (i.e., normalization and nonnegativeness) and yields a smooth and continuous function. In principle, if the gas kinematics are known a priori, the technique can be used to infer spatial distributions at a resolution somewhat higher than that of the beam (see, e.g., Scoville, Young, & Lucy 1983). Here, however, because of the relatively poor signal-to-noise ratio in individual spectra and the lack of detailed knowledge as to the CO kinematics, the model is fitted directly to the velocity-integrated map.

The 21 cm survey of CRW is useful for testing this rectification scheme, because it has the same angular resolution as ours, and because the H I radial distribution is known from higher resolution surveys, which therefore serve as a check. In Figure 9, the solid curves are the H I radial distributions in the southwest and northeast halves of M31 determined by applying the R-L technique to the CRW velocity-integrated map (Fig. 3*a*). In Figure 9*a*, these are compared to the results from a simple binning of the CRW data (after interpolation to a finer grid to eliminate quantization), and in Figure 9*b*, they are compared to a binning of a higher resolution 21 cm survey. It is apparent that the structure seen in the higher resolution profiles is better reproduced by the R-L technique than by simple binning. Some of the discrepancy between the curves in Figure 9*b*, particularly at $R < 6$ kpc, may be attributable to the lack of short-spacing data in the interferometric 21 cm survey used (Unwin 1980). Figure 9*c* demonstrates that the R-L technique yields results which are quite similar to that of χ^2 minimization.

The radial distributions of H_2 surface density for the southwest and northeast halves of M31, and for the galaxy as a whole, are shown by the solid lines in Figures 10*a* to 10*c*, respectively; the dotted ones show the corresponding H I surface densities, scaled down by a factor of 3. The H_2 distributions in the southwest and northeast exhibit the same symmetry that was evident in several previous figures: the main peaks corresponding to the Population I ring are nearly identical in height, width, and galactic radius, and both distributions show evidence for spiral arms beyond the ring (arm 5 of Arp 1964) and inward of the ring (arm 3).

The main peaks in the southwest and northeast H_2 radial distributions occur at the same galactic radius (9.5 kpc) even though in the spatial map (Fig. 3*b*) the southwest tangent of the ring lies at a smaller X (−41′) than the northeast tangent (45′). The southwest tangent is assigned to a larger galactic radius than its position along the major axis would indicate because it is also offset in Y by ∼4′.5 (see § 4.2). This example illustrates that the derived radial distribution depends on the interpretation of the strong peak in the spatial map near (−41′, +4′.5): is it the limb-brightened tangent of a warped Population I ring, or is it largely a true density enhancement at a somewhat larger radius? Figure 10*d* shows the effect on the derived H_2 and H I densities of assuming that the disk on the southwest side is warped. The effect of such a warp on the H_2 distribution is not large: the Population I ring is shifted inward only slightly (compare the relative intensities of the bins at 8.5 and 10.5 kpc). The H I distribution is more dramatically affected, but mainly in the outer arm 5 which is very weak in CO. Figure 10*d* is simply an updated version of Figure 3*b* of Koper et al. (1991); the H I distribution has not changed, but that of H_2 has, owing to the minor changes in the W_{CO} map discussed in § 4.1.

As Figure 10*c* shows, the Population I ring in H_2 is centered ∼1 kpc inward of that in H I. The cause of this offset is probably not a systematic offset between CO and H I within a particular spiral arm, since higher resolution studies (e.g., Stark 1985) have found no such effect; it may instead simply reflect the increase in molecular fraction from the outer to inner edge of the ring noted earlier (§ 4.3). The H_2 mass surface density at the peak of the Population I ring at 9.5 kpc is $\sim 1.3\ M_\odot\ \mathrm{pc}^{-2}$, approximately one-third the H I surface density there. Although the densities of both tracers drop sharply inward of the ring and the CO emission inside of $R = 6$ kpc is very weak, the H_2 and H I densities may be comparable in the inner arm 3 near 4.5 kpc. Beyond the ring, the H_2 density drops very sharply—by about an order of magnitude between 10 and 14 kpc—while the H I density falls by only 10%–20%. The total H_2 mass of M31, on the present assumption of a Galactic X ratio (which Paper II will show to be questionable), is $2.7 \pm 0.2 \times 10^8\ M_\odot$, more than a factor of 10 less than its H I mass ($3.8 \times 10^9\ M_\odot$, derived in the same way from the CRW survey after subtraction of Galactic foreground emission).

Even if the H_2 density at the peak of the Population I ring in M31 is only one-fifth that at the peak of the molecular ring in the Milky Way near 4 kpc, as the Galactic X implies, it is still comparable to the H_2 density *at the same radius* in the Milky Way (Dame et al. 1987). This fact, and the apparent increase in the molecular fraction inward of 10 kpc in both galaxies, may be important clues to the nature of both molecular rings. At and beyond 10 kpc, the two galaxies are rather similar in their molecular and atomic densities, and it may be that the essential difference between the two is that the density of gas in all forms decreases sharply inward of 10 kpc in M31, while here the H I density remains roughly constant and the molecular density continues to increase with decreasing R to about 4 kpc. Possible causes of this difference will be considered in Paper II.

5. SUMMARY

We have used the CfA 1.2 m telescope to carry out the first complete CO survey of M31. This survey was the most difficult and sensitive among the many so far undertaken with that instrument, requiring observations for 8 hr each day during two 6 month observing seasons. Spectra were obtained on the same half-beamwidth grid as that used with the Effelsberg 100 m telescope by Cram et al. (1980) for their 21 cm survey of M31, since the beam of that instrument at 21 cm is nearly

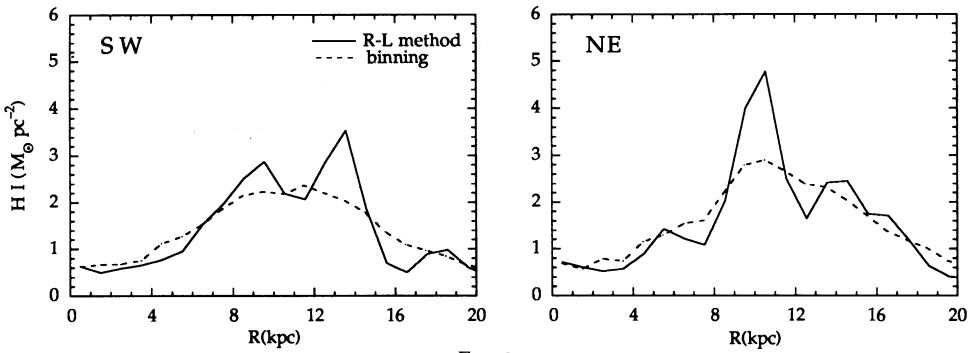

FIG. 9*a*

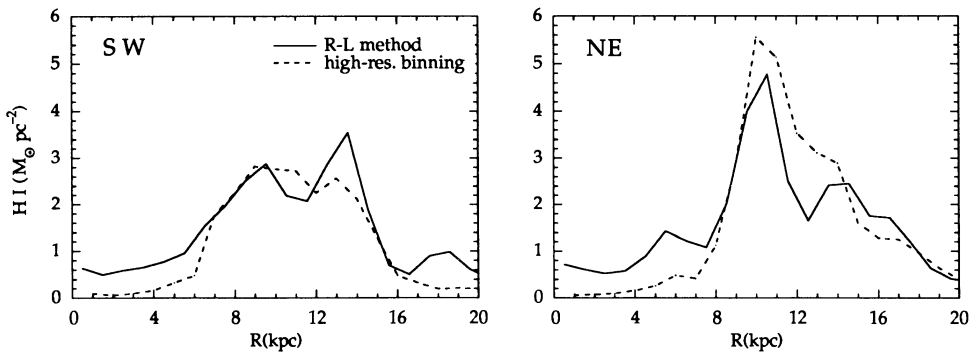

FIG. 9*b*

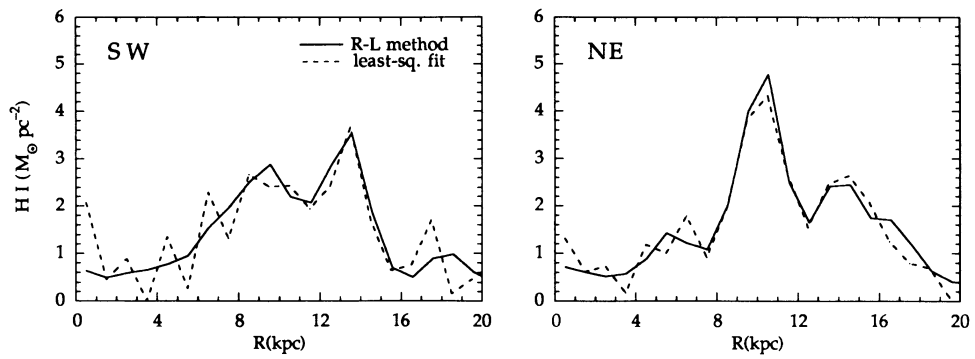

FIG. 9*c*

FIG. 9.—The radial distribution of H I surface density in M31 as determined by the Richardson-Lucy method (*solid curves*) compared with that determined by three other methods (*dotted curves*). Results for the southwest side of the galaxy are shown in the left column, those for the northeast side in the right column. In (*a*), the dotted curves are the result of binning the CRW survey into 1 kpc wide radius bins, after interpolating to a fine grid to eliminate quantization effects. In (*b*), the dotted curves are the result of binning the interferometric 21 cm survey of Unwin (1980), which has an angular resolution of ~1′ (adapted from his Fig. 8). In (*c*), the dotted curves are the result of fitting an inclined, axisymmetric disk to the CRW integrated map using the method of least-squares.

identical to ours at CO. Although few spectra showed CO lines with peak temperatures more than a few times the instrumental noise, extremely flat spectral baselines and broad linewidths resulted in high signal-to-noise ratio in velocity-integrated intensity, and a good determination of the molecular distribution with galactocentric radius.

Most of the CO emission in M31 is confined to a fairly well-defined ring near $R = 10$ kpc, very similar to that seen in other Population I tracers such as H II regions, radio continuum, and far-infrared emission. The molecular gas is similar to the atomic gas in that it peaks in the Population I ring and is very scarce at the galactic center, but differs in its much sharper decrease in density beyond the ring and its clumpier appearance, plausibly the result of a higher arm-interarm contrast for molecular gas than for atomic.

Although the molecular gas and all associated Population I peak in the 10 kpc ring and the surface densities of both atomic and molecular gas decrease sharply within, it is possible that the fraction of gas that is molecular may actually increase. Of particular note is a region at $R = 4.5$ kpc near the tangent of Arp's spiral arm N3 which apparently has an H_2/H I ratio roughly 3 times the mean value in the ring.

At the angular resolution of the present survey, the molecular and atomic gas in M31 appear to have the same large-scale kinematics. Essentially all CO lines are coincident in velocity with corresponding 21 cm lines, although the 21 cm profiles are

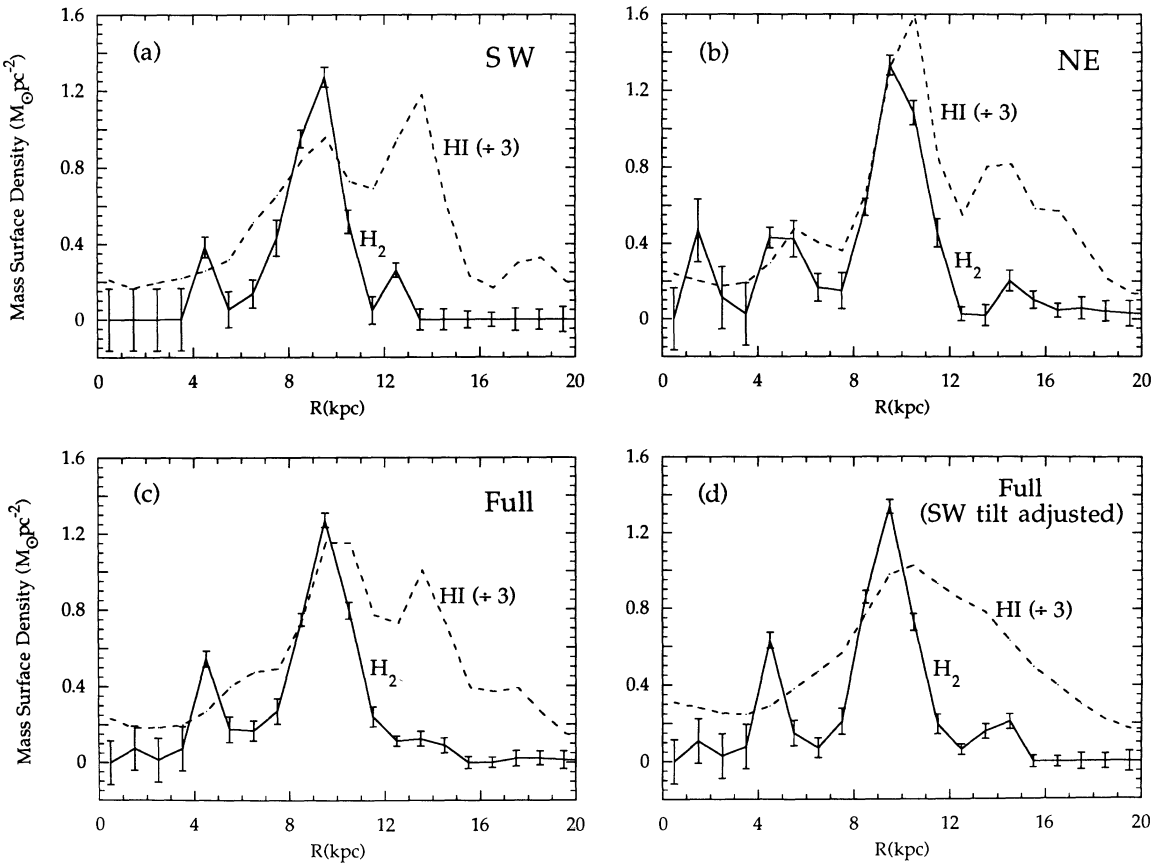

FIG. 10.—Radial distributions of atomic (*dotted*) and molecular (*solid*) mass surface densities in M31, as determined by a Richardson-Lucy fit to the $N_{\rm H\,I}$ and $W_{\rm CO}$ maps in Fig. 3. Molecular column densities were calculated assuming the Milky Way value for the $N(\rm H_2)/W_{\rm CO}$ ratio (see text), a distance of 690 kpc, and a disk inclination of 77°. The error bars represent 1 σ instrumental noise. (*a*) the southwest ($X < 0'$) half of the galaxy; (*b*) the northeast ($X > 0'$) half; (*c*) the entire galaxy; (*d*) the entire galaxy on the assumption that the southwest disk is tilted such that the major axis passes through the point (−45′, 4.′5).

generally more complex, showing additional components not detected in CO. Toward the tangents of the Population I ring, where 21 cm spectra are particularly broad and complex, the CO lines generally correspond to the 21 cm component farthest from the systemic velocity of the galaxy and arising from the inner disk.

REFERENCES

Allen, R. J., & Lequeux, J. 1993, ApJ, 410, L15
Arp, H. 1964, ApJ, 139, 1045
Baade, W., & Arp, H. 1964, ApJ, 139, 1027
Bally, J. 1992, private communication
Beck, R., & Gräve, R. 1982, A&A, 105, 192
Berkhuijsen, E. M. 1977, A&A, 57, 9
Berkhuijsen, E. M., Beck, R., & Gräve, R. 1987, in Interstellar Magnetic Fields, ed. R. Beck & R. Gräve (Berlin: Springer), 38
Berkhuijsen, E. M., & Wielebinski, R. 1974, A&A, 34, 173
Blitz, L. 1985, ApJ, 296, 481
Boulanger, F., Stark, A. A., & Combes, F. 1981, A&A, 93, L1
Braun, R. 1991, ApJ, 372, 54
Brinks, E., & Shane, W. W. 1984, A&AS, 55, 179
Bronfman, L., Cohen, R. S., Alvarez, H., May, J., Thaddeus, P. 1988, ApJ, 324, 248
Casoli, F. 1991, in Dynamics of Galaxies and Their Molecular Cloud Distributions, ed. F. Combes & F. Casoli (Dordrecht: Kluwer), 51
Combes, F., Encrenaz, P. J., Lucas, R., & Weliachew, L. 1977, A&A, 61, L7
Cram, T. R., Roberts, M. S., & Whitehurst, R. N. 1980, A&AS, 40, 215 (CRW)
Dame, T. M. 1993, in Back to the Galaxy, ed. S. Holt & F. Verter (New York: AIP Press), 267
Dame, T. M., Elmegreen, B. G., Cohen, R. S., & Thaddeus, P. 1986, ApJ, 305, 892
Dame, T. M., Koper, E., Israel, F. P., & Thaddeus, P. 1991, in Dynamics of Galaxies and Their Molecular Cloud Distributions, ed. F. Combes & F. Casoli (Dordrecht: Kluwer), 23
Dame, T. M., et al. 1987, ApJ, 322, 706
Davis, J. H., & Vanden Bout, P. 1973, Ap. Letters, 15, 43
Dickman, R. L. 1978, ApJS, 37, 407
Digel, S. W. 1991, Ph.D. thesis, Harvard Univ.
D'Odorico, S., Dopita, M. A., & Benvenuti, P. 1980, A&AS, 40, 67
Emerson, D. T. 1974, MNRAS, 169, 607
Grabelsky, D. A., Cohen, R. S., Bronfman, L., & Thaddeus, P. 1988, ApJ, 331, 181
Habing, H. J., et al. 1984, ApJ, 278, L59
Henderson, A. P. 1979, A&A, 75, 311
Hjellming, R. M., & Smarr, L. L. 1982, ApJ, 257, L13
Hodge, P. 1992, The Andromeda Galaxy (Dordrecht: Kluwer)
Koper, E., Dame, T. M., Israel, F. P., & Thaddeus, P. 1991, ApJ, 383, L11
———. 1993, in preparation (Paper II)
Kutner, M. L. 1978, Ap. Letters, 19, 81
Lucy, L. B. 1974, AJ, 79, 745
Mauzy, B. 1974, NRAO Electronics Div. Internal Rept., No. 146
Pan, S.-K., Kerr, A. R., Feldman, M. J., Kleinsasser, A. W., Stasiak, J. W., Sandstrom, R. L., & Gallagher, W. J. 1989, IEEE Trans., MTT-37, 580
Pellet, A., Astier, N., Viale, A., Courtès, G., Maucherat, A., Monnet, G., & Simien, F. 1978, A&AS, 31, 439
Rickard, L. J., Palmer, P., Morris, M., Turner, B. E., & Zuckerman, B. 1977, ApJ, 213, 673
Roberts, M. S. 1966, ApJ, 144, 639
Ryden, B. S., & Stark, A. A. 1986, ApJ, 305, 823
Sandqvist, Aa., Elfhag, T., & Lindblad, P. O. 1989, A&A, 218, 39
Scoville, N. Z., Young, J. S., & Lucy, L. B. 1983, ApJ, 270, 443
Solomon, P. M., & de Zafra, R. 1975, ApJ, 199, L79
Solomon, P. M., Rivolo, A. R., Barrett, J. W., & Yahil, A. 1987, ApJ, 319, 730
Stark, A. A. 1979, Ph.D. thesis, Princeton Univ.
———. 1985, in The Milky Way Galaxy, ed. H. van Woerden, R. J. Allen, & W. B. Burton (Dordrecht: Reidel), 445
Stark, A. A., Linke, R. A., & Frerking, M. A. 1981, BAAS, 13, 535
Strong, A. W., et al. 1988, A&A, 207, 1
Unwin, S. C. 1980, MNRAS, 192, 243
Walterbos, R. A. M. 1986, Ph.D. thesis, Leiden Univ.
Walterbos, R. A. M., & Schwering, P. B. W. 1987, A&A, 180, 27